Oscillatory Electro-oxidation of Methanol on Nanoarchitectured Pt$_{pc}$/Rh/Pt Metallic Multilayer

Raphael Nagao,[†,‡,⊥] Renato G. Freitas,[†,§] Camila D. Silva,[†] Hamilton Varela,[‡,∥] and Ernesto C. Pereira[*,†]

[†]Department of Chemistry, Federal University of São Carlos, P.O. Box 676, 13565-905 São Carlos, São Paulo, Brazil
[‡]Institute of Chemistry of São Carlos, University of São Paulo, P.O. Box 780, 13560-970 São Carlos, São Paulo, Brazil
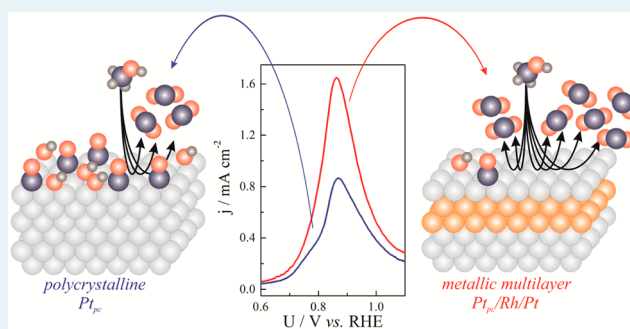[§]Department of Chemistry, Federal University of Mato Grosso, 78060-900 Cuiaba, Mato Grosso, Brazil
[∥]Ertl Center for Electrochemistry and Catalysis, GIST, Cheomdan-gwagiro 261, Buk-gu, Gwangju 500-712, South Korea

Ⓢ *Supporting Information*

ABSTRACT: The oscillatory electro-oxidation of methanol was studied on polycrystalline Pt$_{pc}$ and Pt$_{pc}$/Rh$_{2.0}$/Pt$_{1.0}$ metallic multilayers. The surfaces investigated consisted of 1.0 Pt outlayer surface deposited onto 2.0 Rh intralayers beneath a Pt outlayer and over the polycrystalline Pt$_{pc}$ substrate. In addition to experimental studies, numerical simulations were performed using a dimensionless kinetic model for the electro-oxidation of methanol in order to provide a better understanding of the role played by the nanostructured metallic multilayer electrode in the electrocatalytic activity. A comparable electrochemical behavior found for cyclic voltammetry in blank acidic media was observed in both electrodes. Remarkably, an increase of 90% in the peak current density around 0.88 V vs. RHE in the electro-oxidation of methanol appeared when Pt$_{pc}$/Rh$_{2.0}$/Pt$_{1.0}$ was utilized. The numerical simulations suggested that this increase in the electrocatalytic activity for the metallic multilayer electrode is due to the prevention of carbon monoxide adsorption on the surface and a consequent increase in the production of carbon dioxide from the direct pathway. Indeed, a decrease in the reaction rate constant of carbon monoxide formation resulted in an increase of the current density associated with CO_2 formation in the potentiodynamic sweep, in addition to the decrease in amplitude and frequency of the oscillatory time series. As the rate of carbon monoxide adsorption is suppressed by the presence of the metallic multilayers, the intrinsic drift usually found in the oscillatory electro-oxidation of methanol was enhanced and oscillations ceased earlier. Overall, the combination of electrochemical experiments and numerical simulations suggests that carbon monoxide acts as a poisoning species instead of a reaction intermediate in the electro-oxidation of methanol.

KEYWORDS: *oscillations, metallic multilayer, methanol, electrocatalysis*

1. INTRODUCTION

The search for more selective and efficient catalysts for complete electro-oxidation of methanol has been an active field of research in the past few decades due to the possibility of using fuel cells as a green and renewable energy source.[1,2] Several methodologies have been employed in order to enhance the catalytic activity by modifications in their structural properties; among them, the use of alloys, electrodeposits, and nanoparticles has been shown to be quite promising in this direction.[3–6] Metallic multilayers are a new class of advanced engineered materials that are known to exhibit high structural stability, mechanical strength, high ductility, toughness, and resistance to fracture and fatigue.[7] Moreover, this class has been widely explored mainly due to its magnetic properties.[8,9] From the perspective of electrocatalysis, Pereira and co-workers[10–16] have extensively studied the preparation and characterization of metallic multilayers deposited onto polycrystalline platinum (Pt$_{pc}$) as catalysts for the electro-oxidation of small organic molecules.

For instance, the authors observed that, although the Pt$_{pc}$/Metal/Pt (Metal = Rh, Ru, Bi, Ir) electrode has a Pt outlayer surface, the electrocatalytic activity for such metallic multilayers is higher than that observed for the Pt$_{pc}$ electrode. Oliveira et al.[10] experimentally observed increases in the peak current density of between about 2 and 4 times for the electro-oxidation of methanol, ethanol, formaldehyde, and formic acid on Pt$_{pc}$/Rh/Pt with respect to that on Pt$_{pc}$. Interestingly, a highly selective oxidation of ethanol to carbon dioxide was obtained when the reaction was carried out on a Pt$_{pc}$/Ir/Pt nanostructured electrode,[14] as reflected in the absence of the infrared bands relative to acetic acid and acetaldehyde molecules.

In spite of much effort devoted to this topic, the role played by metallic multilayer electrodes in the improvement of

electrocatalytic activity is not completely understood. Herein we provide some mechanistic evidence, based on a combination of experiments, modeling, and numerical simulations, under both conventional and oscillatory regimes, that the increase in the current density observed in the electro-oxidation of methanol over the metallic multilayer electrode is mainly caused by the production of carbon dioxide from the oxidative decomposition of the active intermediate: i.e., the direct pathway. This argument is supported by the highly selective electronic effect caused by nanostructured metallic multilayers in preventing the adsorption of carbon monoxide. Potential oscillations registered under galvanostatic control were utilized as a mechanistic probe, corroborating the scenario of suppression of adsorbed carbon monoxide.
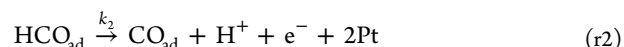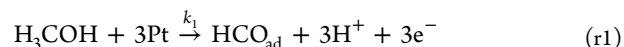
2. EXPERIMENTAL SECTION

Solutions were prepared using ultrapure water (Millipore, 18.2 MΩ cm), $HClO_4$ (Sigma-Aldrich, 70%), H_2SO_4 (Mallinckrodt, 99.8%), $RhCl_3 \cdot 3H_2O$ (Alfa-Aesar, 99.9%), $H_2PtCl_6 \cdot 6H_2O$ (Sigma-Aldrich, 99.9%), and H_3COH (J. T. Baker, 99.9%). The electrochemical cell, all glassware, and electrodes were cleaned in a solution of $KMnO_4$ and $NaOH$ for 12 h. Subsequently, all electrochemical apparatus were soaked for 1 h in a bath of H_2O_2 and H_2SO_4 concentrated solution. Finally, the systems were carefully and exhaustively rinsed with ultrapure water and boiled in it at least three times. This cleaning procedure resulted in voltammograms free from any impurities.

In order to prepare the metallic multilayer electrode, a polycrystalline Pt_{pc} (0.3 cm^2, Sigma-Aldrich, 99.99%) substrate was utilized. It was mechanically polished with diamond paste down to 1.0 μm and washed with acetone and a large amount of ultrapure water. The potential of deposition was 0.05 V (vs a reversible hydrogen electrode, RHE) for 1800 and 120 s leading to about 2.0 and 1.0 Rh and Pt monolayers (MLs), respectively. The procedure was as follows: Rh intralayer was electrodeposited from the precursor solution, 2.0×10^{-5} mol L^{-1} of $RhCl_3 \cdot 3H_2O$ in 0.1 mol L^{-1} of $HClO_4$, and the charge related to the electrodeposition process was used to obtain the number of Rh MLs. After that, the electrode was washed carefully in ultrapure water and transferred to another electrochemical cell with 5.0×10^{-4} mol L^{-1} of $H_2PtCl_6 \cdot 6H_2O$ solution in 0.1 mol L^{-1} of $HClO_4$, where the Pt outlayer could be electrodeposited, leading to $Pt_{pc}/Rh_{2.0}/Pt_{1.0}$ nanostructured electrodes.
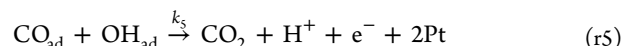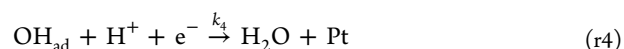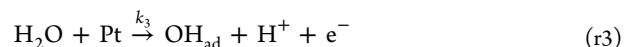
The electrochemical characterization of the metallic multilayer electrodes was carried out using a Autolab PGSTAT 302N potentiostat/galvanostat equipped with a SCANGEN module. Voltammetric curves were measured in 0.5 mol L^{-1} of H_2SO_4 solution in the potential range between 0.05 and 1.40 V. A platinized-Pt plate (Sigma-Aldrich, 99.99%) was used as the auxiliary electrode. Prior to the experiments, the solutions were sparged with N_2 (White Martins, 5 N) for 30 min. The electrolyte was kept free of atmospheric pollutant gas by continuously introducing N_2 into the region of the electrochemical cell above the electrolyte. Prior to each galvanostatic time series, the working electrode was cycled between 0.05 and 1.40 V in 0.5 mol L^{-1} of H_3COH and 0.5 mol L^{-1} of H_2SO_4 for 30 cycles. Soon after, the galvanostatic time series for several current values were recorded.

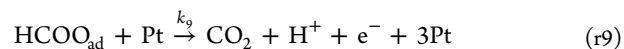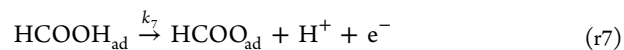## 3. MODELING THE ELECTRO-OXIDATION OF METHANOL

Electrochemical experiments were compared to numerical simulations in order to shed light on some mechanistic aspects in the electro-oxidation of methanol on the modified surfaces. The modeling procedure was based on 10 elementary steps, r1−r10, in a dimensionless model previously proposed by Nagao et al.[17] As is widely accepted, the electro-oxidation of methanol proceeds through the so-called dual pathway mechanism.[18] The indirect pathway is described by the adsorption of the methanol molecule with consecutive dehydration steps, which results in the formation of adsorbed carbon monoxide:[19,20] i.e., CO_{ad}. See steps r1 and r2, respectively.

$$H_3COH + 3Pt \xrightarrow{k_1} HCO_{ad} + 3H^+ + 3e^- \tag{r1}$$

$$HCO_{ad} \xrightarrow{k_2} CO_{ad} + H^+ + e^- + 2Pt \tag{r2}$$

In our model we considered only the formation of OH_{ad} as the oxygenated species by the oxidation of water. In this case, step r3 represents the oxidation reaction while r4 is related to the reduction one. This simplification has been used successfully in different modeling procedures for the electro-oxidation of small organic molecules.[17,21,22] In addition, CO_{ad} reacts with adsorbed oxygenated species in a Langmuir−Hinshelwood mechanism, step r5, resulting in CO_2.[23]

$$H_2O + Pt \xrightarrow{k_3} OH_{ad} + H^+ + e^- \tag{r3}$$

$$OH_{ad} + H^+ + e^- \xrightarrow{k_4} H_2O + Pt \tag{r4}$$

$$CO_{ad} + OH_{ad} \xrightarrow{k_5} CO_2 + H^+ + e^- + 2Pt \tag{r5}$$

Occurring in parallel, the direct pathway takes place by the formation of soluble products, such as formic acid and formaldehyde, which can also form CO_2 from the oxidative decomposition of the active intermediates,[24−26] and methyl formate, which is easily detected by means of differential electrochemical mass spectrometry (DEMS).[27−29] The nature of the active intermediate is still under debate, but it is currently believed to proceed by a very fast path.[30] In this context, we adopted the production of adsorbed formate, i.e. $HCOO_{ad}$ in step r7, as the active intermediate formed only from formic acid dehydration, and ignored the formation of $HCOOCH_3$ by the homogeneous reaction between $HCOOH$ and H_3COH in solution[27] and the esterification reaction between HCO_{ad} and H_3COH.[29] Nevertheless, methyl formate can be followed by HCO_{ad} time evolution, as it is a precursor to its formation.[17]

$$HCO_{ad} + Pt + H_2O \xrightarrow{k_6} HCOOH_{ad} + H^+ + e^- + 2Pt \tag{r6}$$

$$HCOOH_{ad} \xrightarrow{k_7} HCOO_{ad} + H^+ + e^- \tag{r7}$$

$$HCOO_{ad} + H^+ + e^- \xrightarrow{k_8} HCOOH_{ad} \tag{r8}$$

$$HCOO_{ad} + Pt \xrightarrow{k_9} CO_2 + H^+ + e^- + 3Pt \tag{r9}$$

We attributed steps r6−r9, as also being responsible for the production of CO_2 derived from the readsorption process of soluble species. In this case, only formic acid is incorporated in the model and all molecules can form adsorbed formate. An

excellent agreement between experiments and simulations based on these assumptions was recently observed.[31] Finally, formic acid might also result in CO_{ad} from a reduction step of $HCOO_{ad}$, as proposed by Cuesta et al.[32]

$$HCOO_{ad} + Pt + H^+ + e^- \xrightarrow{k_{10}} CO_{ad} + H_2O + 2Pt \tag{r10}$$
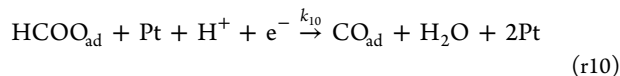
Each coverage variable was converted in the generic representation x_n according to $x_2 = \theta_{HCO}$, $x_3 = \theta_{OH}$, $x_4 = \theta_{CO}$, $x_5 = \theta_{HCOOH}$, and $x_6 = \theta_{HCOO}$; $x_e = e^{\omega\phi}$ is the electrical component for Faradaic reactions, and ω is the transfer coefficient. The surface free sites are denoted as x_1 and can be written as

$$x_1 = 1 - 3x_2 - x_3 - x_4 - 2x_5 - 2x_6$$

On application of the kinetic laws in each elementary step, we obtain

$$v_1 = k_1 x_1^2 x_e \tag{e1}$$

$$v_2 = k_2 x_2 x_e \tag{e2}$$

$$v_3 = k_3 x_1 x_e \tag{e3}$$

$$v_4 = k_4 x_3 x_e^{-1} \tag{e4}$$

$$v_5 = k_5 x_3 x_4 x_e \tag{e5}$$

$$v_6 = k_6 x_1 x_2 x_e \tag{e6}$$

$$v_7 = k_7 x_5 x_e \tag{e7}$$

$$v_8 = k_8 x_6 x_e^{-1} \tag{e8}$$

$$v_9 = k_9 x_1 x_6 x_e \tag{e9}$$

$$v_{10} = k_{10} x_1 x_6 x_e^{-1} \tag{e10}$$

Additional simplifications such as the assumption of two free active sites[33] in eq e1 and the independence of the number of electrons produced in x_e were adopted and, as previously observed, do not result in significant changes in comparison to experimental observations.[17,34] Hence, the electrochemical model can be written as a set of six autonomous ordinary differential equations, e11−e16

$$\dot{x}_2 = v_1 - v_2 - v_6 \tag{e11}$$

$$\dot{x}_3 = v_3 - v_4 - v_5 \tag{e12}$$

$$\dot{x}_4 = v_2 - v_5 + v_{10} \tag{e13}$$

$$\dot{x}_5 = v_6 - v_7 + v_8 \tag{e14}$$

$$\dot{x}_6 = v_7 - v_8 - v_9 - v_{10} \tag{e15}$$

$$\dot{\phi} = i - v_F \tag{e16}$$

with

$$v_F = 3v_1 + v_2 + v_3 - v_4 + v_5 + v_6 + v_7 - v_8 + v_9 - v_{10} \tag{e17}$$

$$i = \frac{u - \phi}{r} \tag{e18}$$

In eq e18, i might be interpreted as the total current, u as the applied potential, and r as the ohmic drop between the working and reference electrodes. The six ordinary differential equations

were numerically integrated using the tool ode15s in the Matlab software. When not specified, the initial conditions were considered as 0.

4. RESULTS AND DISCUSSION

Figure 1 depicts the electrochemical characterization carried out by linear potentiodynamic sweeps at $dU/dt = 0.10$ V s^{-1} on

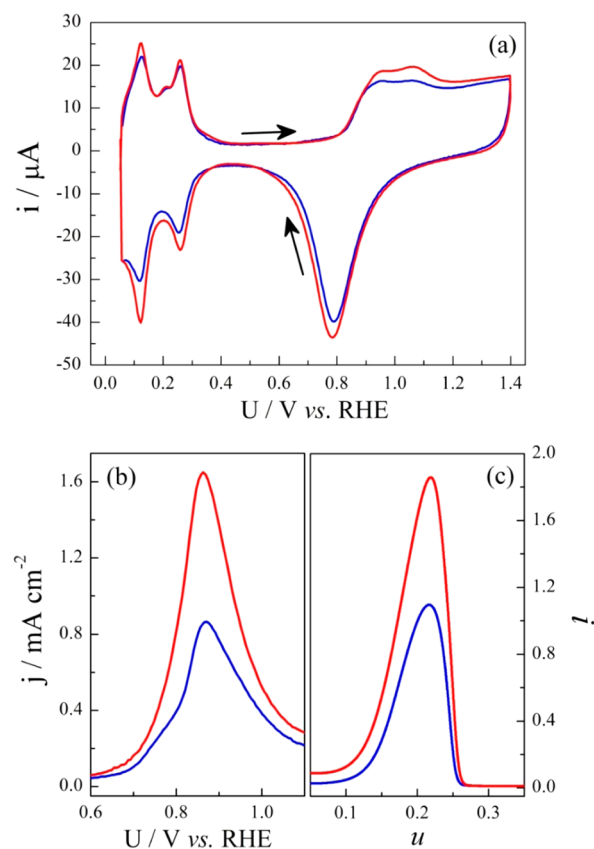**Figure 1.** (a) Cyclic voltammetry at $dU/dt = 0.10$ V s^{-1} under Pt_{pc} (blue curves) and $Pt_{pc}/Rh_{2.0}/Pt_{1.0}$ (red curves) in sulfuric acidic media. Potential linear sweep at the same rate measured in (b) electrochemical experiments and (c) numerical calculations in the electrooxidation of methanol. $k_2 = 5.0$ and $k_3 = 1.0$ (blue curve); $k_2 = 0.7$ and $k_3 = 0.9$ (red curve) in numerical simulations at $du/dt = 0.01$, $u(0) = -0.3$, and $x_4(0) = 0.9$. Additional parameters are $k_1 = 6.0$, $k_4 = 4.0$, $k_5 = 0.079$, $k_6 = 50$, $k_7 = 600$, $k_8 = 30$, $k_9 = 300$, $k_{10} = 0.1$, $\omega = 15$, and $r = 0.05$.

a polycrystalline platinum electrode, with Pt_{pc} depicted by the blue curves and the nanostructured metallic multilayer electrode $Pt_{pc}/Rh_{2.0}/Pt_{1.0}$ as the red curves; experiments were performed in 0.1 mol L^{-1} sulfuric acid in the (Figure 1a) absence and (Figure 1b) presence of 0.5 mol L^{-1} methanol. Numerical simulations presented in Figure 1c were performed at $du/dt = 0.01$ with changes in k_2 and k_3 in order to qualitatively reproduce the experimental observations. In this case, the set of reaction rate constants $k_2 = 5.0$ and $k_3 = 1.0$ represents the blue curves and the set $k_2 = 0.7$ and $k_3 = 0.9$ represents the red curves.

Typical voltammetric behavior can be observed in Figure 1a for Pt_{pc} and $Pt_{pc}/Rh_{2.0}/Pt_{1.0}$ electrodes in sulfuric acid solution,[35] where the electrochemical process in the cyclic voltammograms can be associated with (i) hydrogen adsorption and desorption between 0.05 and 0.40 V, (ii) double-layer

region between 0.40 and 0.80 V, and (iii) formation and reduction of platinum oxides, between 0.80 and 1.40 V and between 1.4 and 0.40 V, respectively. As is evident in Figure 1a, the voltammetric profile for polycrystalline platinum is thoroughly recovered when the $Pt_{pc}/Rh_{2.0}/Pt_{1.0}$ structure is formed by the deposition of a Pt layer over the Rh surface, which implies a surface composed mostly by platinum atoms. XPS measurements have confirmed this experimental evidence.[10,12] The electrochemical surface areas for Pt_{pc} and $Pt_{pc}/Rh_{2.0}/Pt_{1.0}$ electrodes were calculated by using the well-established procedure in the literature,[36] which considers a charge density of 210 $\mu C\ cm^{-2}$ as being equivalent to desorption of one hydrogen monolayer. The electrochemical surface areas for Pt_{pc} and $Pt_{pc}/Rh_{2.0}/Pt_{1.0}$ electrodes differ by about 5%, and then all current densities were normalized by their values. These results are in agreement with in situ AFM experiments which revealed the same roughness mean square values for both electrodes.[11−13]

On analysis of the electro-oxidation of methanol over Pt_{pc} and $Pt_{pc}/Rh_{2.0}/Pt_{1.0}$ electrodes in Figure 1b, an increase of ca. 90% was observed in the peak current density for $Pt_{pc}/Rh_{2.0}/Pt_{1.0}$ along the linear potentiodynamic sweep. Similar behavior of the increased catalytic activity in the electro-oxidation of different small organic molecules has been showed by Pereira and co-workers.[10−16] As commonly accepted, the electro-oxidation of methanol proceeds through parallel pathways,[18] as already presented in section 3. One controversial point to be stressed is the role played by carbon monoxide during the electro-oxidation process. Due to its strong influence on fuel cell efficiency, it has triggered a continuous study of its removal at low potentials by the presence of different metals such as Ru, Rh, Sn, etc.[37−39] In the literature, a great deal of effort has been made in the development of more selective catalysts based on the bifunctional mechanism and electronic effects.[40−43]

Considering the absence of Rh adatoms in the surface of a metallic multiyear electrode, justified by the lack of observation of the characteristic bands of the second metal in XPS measurements[10,12] and the similarity between the profiles for the hydrogen underpotential deposition in the cyclic voltammetry in Figure 1a, the mechanism that would explain the experimental results in Figure 1b might be attributed to (a) the electronic interaction of the exposed Pt outlayer and the Rh interlayer beneath, weakening the back-donation between the CO antiligand orbitals 2π*, with energies above the Fermi level, and the d-band from the Pt outlayer[42,43] and (b) the compressive strain due to the electrodeposition of a monolayer between two distinct substrates and interatomic distances, resulting in an enlargement of the d-band and, consequently, lower energies of adsorption.[44,45] Both electronic effects can, indeed, prevent the formation of CO_{ad} on the surface. Experimental results have showed the catalytic effect of Rh for the electro-oxidation of methanol,[10,38,46] but as previously discussed, in this set of results we can discard the contribution from the bifunctional mechanism and the formation of rhodium oxides.

Numerical simulations were also carried out, and a good correspondence with the electrochemical measurements was obtained when the reaction rate constants of formation of adsorbed CO_{ad} and OH_{ad} were changed, as can be seen in Figure 1c. Although the suppression of carbon monoxide layer formation is enhanced in the presence of a metallic multilayer electrode, interestingly, just a slight shift in the current density peak for more negative potentials has been observed. According

to our simulations, this behavior can be mostly attributed to a decrease in k_2 values, which results in an increase of catalytic activity, while k_3 affected drastically the potential range where the maximum current occurs (see Figure S1 in the Supporting Information for additional details). Hence, the enhancement of the catalytic activity in the electro-oxidation of methanol might be understood in terms of the removal of carbon monoxide from the surface.

Galvanostatic experiments were carried out with different applied currents and concomitantly compared with numerical simulations. In Figure 2, potential time series measured at j =
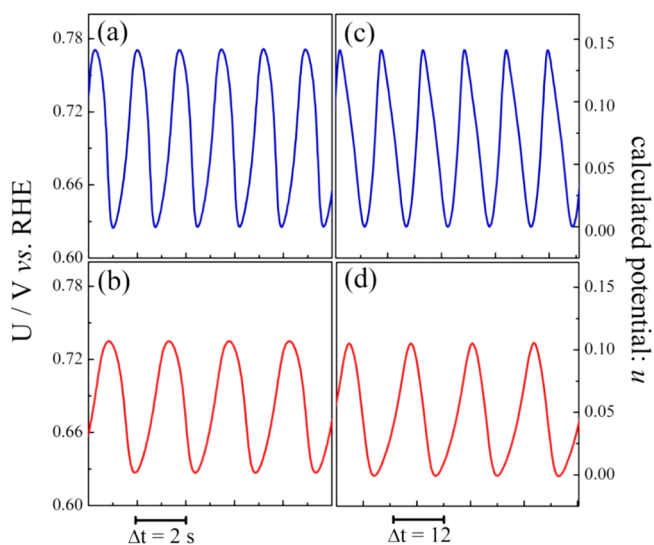

Figure 2. Experimental (a, b) and calculated (c, d) potential time series in the electro-oxidation of methanol at j = 0.32 mA cm^{-2} and i = 0.20, respectively. The blue curves represent Pt_{pc} and k_2 = 5.0, k_3 = 1.0, k_6 = 50, and red curves represent $Pt_{pc}/Rh_{2.0}/Pt_{1.0}$ and k_2 = 0.5, k_3 = 0.8, k_6 = 23; working electrodes in electrochemical experiments and numerical simulations. Additional parameters are k_1 = 6.0, k_4 = 4.0, k_5 = 0.079, k_7 = 600, k_8 = 30, k_9 = 300, k_{10} = 0.1, and ω = 15.

0.32 mA cm^{-2} on (a) Pt_{pc} (blue curves) and (b) $Pt_{pc}/Rh_{2.0}/Pt_{1.0}$ (red curves) working electrodes were compared with numerical simulations at i = 0.20 with (c) k_2 = 5.0, k_3 = 1.0, k_6 = 50 (blue curves) and (d) k_2 = 0.5, k_3 = 0.8, k_6 = 23 (red curves).

Electrochemical oscillations presented the usual profile described in the literature.[47,48] As observed in Figure 2, a good adjustment between experiments and simulations was obtained when the formations of CO_{ad} and OH_{ad} were disfavored. This reinforces the evidence that the metallic multilayer electrode might prevent more selectively the formation of carbon monoxide on the surface. Additionally, qualitative agreement was even improved when k_6 values were decreased from 50 to 23. In spite of a significant increase of the current density in voltammetric experiments, the electrochemical variables do not reveal explicitly the presence of the second metal; nevertheless, some hints become clearly evident in the oscillatory regime. As has already been pointed out, a rich variety of dynamic behavior found during the electrochemical oscillations might be used to extract mechanistic information, such as reaction rate constants.[49] In this specific case, the amplitude shift for lower potential values followed by the decrease of the period is a good indication of surface modification by a second metal.[50,51]

The experimental and numerical results support the proposition that the oxidation of adsorbed carbon monoxide by oxygenated species in a Langmuir–Hinshelwood mechanism is not the predominant reaction step for the CO_2 formation and, consequently, the Faradaic current. In other words, our results suggest that adsorbed carbon monoxide acts as a poisoning species instead of a reaction intermediate in the electro-oxidation of methanol in a wide potential window. This hypothesis has already been investigated[52−54] and is in agreement with our observations. This controversial behavior exhibited by carbon monoxide has been discussed with the aid of spectroscopic and spectrometric techniques coupled in the electrochemical cell.[52−59] The classification as a reaction intermediate was attributed to the high sensitivity of CO_2 production to different anions present in the electrolyte. As the formation of adsorbed carbon monoxide by the surface dehydration of methanol requires a larger number of active sites, CO oxidation was considered a non-negligible elementary step in the overall carbon dioxide production:[56−58] e.g. above approximately 0.6 V vs RHE. In contrast, recent results have showed a strong impact of soluble intermediates in the total production of CO_2 and the Faradaic current.[31,60,61] In fact, Nagao et al.[34] have demonstrated that sulfate anions in the electrolyte impede the CO_2 production more effectively from the direct pathway in comparison to the indirect pathway during the oscillatory electro-oxidation of methanol.

On the basis of these considerations, we utilized modeling and numerical simulations to get some insight into the relative weight of production of CO_2 from the direct and indirect pathways. Figure 3 shows the production of CO_2 from the elementary steps r5 and r9 in the (a) linear sweeps described in Figure 1c and (b) potential time series in Figure 2c,d. Table 1 depicts a more quantitative relationship of Figure 3 in terms of the maximum current found in the linear potential sweep and the mean production during the oscillations.

Under potentiodynamic control (see Figure 3a1−a3), the decrease of the reaction rates k_2 and k_3 resulted in a substantial increase of the formation of CO_2, represented by $v_5 + v_9$, from 0.230 to 0.335, which is in agreement with Figure 1b,c. However, the enhancement in the electrocatalytic activity is clearly related to the higher contribution from the direct pathway. It is mainly occasioned by the prevention of CO_{ad} adsorption, releasing free sites to the oxidative decomposition of the active intermediate. Otherwise, under oscillatory conditions (Figure 3b1−b3), the decrease of k_2 and k_3 also resulted in an inversion of the global contribution of CO_2 formation: a decrease of v_5 from 0.020 to 0.007 and a consequent increase of v_9 from 0.012 to 0.025, respectively. Nevertheless, dramatic changes in the mean production are not exhibited (see Table 1 for a more detailed description). Differently from what is observed in electrochemical experiments coupled with a mass spectrometer,[17,31,34] these oscillations do not end up with CO_2 peak splitting. Harmonic oscillations, favored in lower applied currents, tend to generate period 1 carbon dioxide time series, instead of relaxation ones, where periods 3 and 4 have been observed.[17,31,34]

The removal of carbon monoxide from the surface seems to be the key parameter to increase the activity. Clearly, the metallic multilayer is very efficient for this purpose. This idea was also tested using the electrochemical oscillations in long-term dynamics as a probe to infer the reaction mechanism. A general overview of the effect of $Pt_{pc}/Rh_{2.0}/Pt_{1.0}$ working
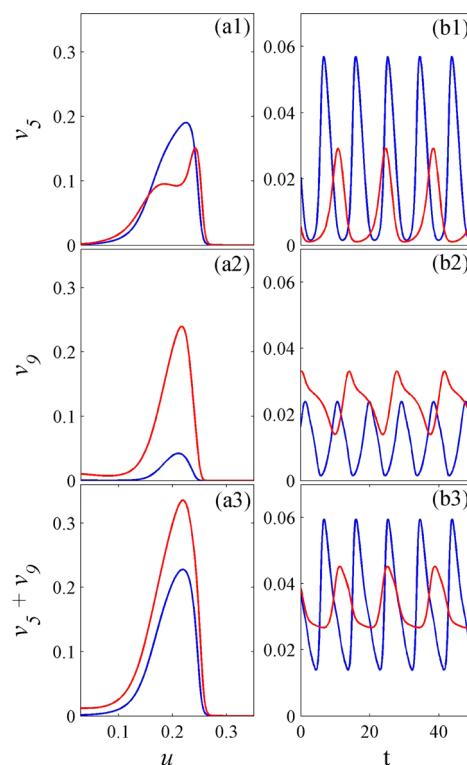

Figure 3. (a) Simulated linear sweeps: $k_2 = 5.0$ and $k_3 = 1.0$ (blue curves); $k_2 = 0.7$ and $k_3 = 0.9$ (red curves); both at $k_6 = 50$, $du/dt = 0.01$, $u(0) = −0.3$, and $x_4(0) = 0.9$. (b) Potential time series: $k_2 = 5.0$, $k_3 = 1.0$, and $k_6 = 50$ (blue curves); $k_2 = 0.5$, $k_3 = 0.8$, and $k_6 = 23$ (red curves); both at $i = 0.20$. Additional parameters are $k_1 = 6.0$, $k_4 = 4.0$, $k_5 = 0.079$, $k_7 = 600$, $k_8 = 30$, $k_9 = 300$, $k_{10} = 0.1$, $\omega = 15$, and $r = 0.05$.

Table 1. Relative Production of Carbon Dioxide Extracted from Figure 3

	v_5		v_9		$v_5 + v_9$	
	blue	red	blue	red	blue	red
max current in linear potential sweep	0.190	0.151	0.042	0.240	0.230	0.335
mean production during oscillations	0.020	0.007	0.012	0.025	0.032	0.032

electrode in the oscillatory electro-oxidation of methanol is better visualized in Figure 4.

The oscillatory period and amplitude were accounted for as a function of the number of cycles over Pt_{pc} and $Pt_{pc}/Rh_{2.0}/Pt_{1.0}$ surfaces and under different applied current densities: e.g., $j = 0.32$, 0.48, 0.64, and 0.81 mA cm$^{−2}$. Overall, the period and amplitude were influenced by either the variation in applied current or the use of a metallic multilayer electrode. As observed in Figure 4, a decrease of j resulted in slower oscillations with smaller amplitudes, while the use of the $Pt_{pc}/Rh_{2.0}/Pt_{1.0}$ electrode enhanced this behavior in all ranges of current densities studied. In contrast to previous experimental findings,[62] the relation between period and amplitude in the oscillatory electro-oxidation of methanol does not seem to be straightforward. This aspect is very important and will be discussed later with the aid of numerical simulations.

Another interesting effect of the nanostructured metallic multilayer electrode in the oscillations is the temporal stability of the time series. Perini et al.[51] have demonstrated a highly
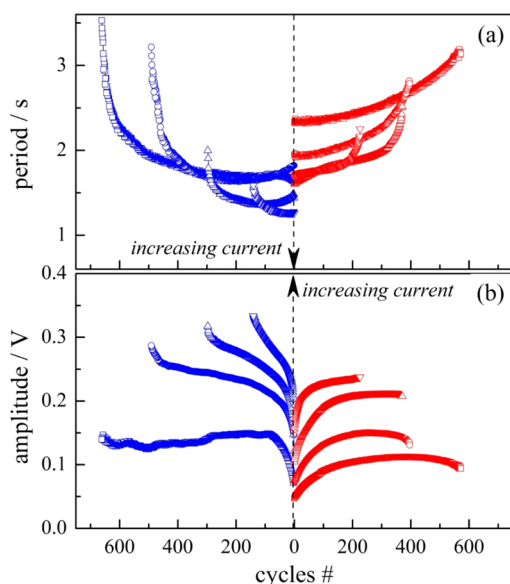
Figure 4. Period (a) and amplitude (b) of the galvanostatic oscillations experimentally measured as a function of the number of cycles in the electro-oxidation of methanol over Pt_{pc} (blue curves) and $Pt_{pc}/Rh_{2.0}/Pt_{1.0}$ (red curves). The dashed arrow indicates the direction of the applied current density from the lowest to the highest values: $j = 0.32$, 0.48, 0.64, and 0.81 mA cm^{-2}.

efficient way to attenuate the intrinsic drift during potential oscillations in the electro-oxidation of formic acid using Sn as a second metal on the surface. The authors were able to keep a robust time series for a very long period of time: e.g., 40 h. On the basis of mechanistic considerations, the rationalized method was performed with the aim of preventing $O_{sub}Pt$ (sub denotes subsurface oxygen[35]) formation, in turn leading to Sn as the main species responsible in forming oxides that might be used in the oxidation with carbonaceous species. The efficiency of the $Pt_{pc}/Rh_{2.0}/Pt_{1.0}$ electrode toward the stabilization of the time series in the electro-oxidation of methanol was analyzed as well. Table 2 summarizes some experimental data collected in Figure 4 as the measured drift in terms of $\Delta U_m[\Delta(cycles)]^{-1}$ and the total number of cycles. Both were reproduced by numerical simulations. In this set of results the drift was simulated by a linear increase of the applied current from an

initial i value of 0.05 and rates of 2.00×10^{-3} and 2.24×10^{-3}. This characteristic has been proved experimentally.[48,63]

As observed in all experimental results with constant applied current, the drift seems to evolve more quickly in the Pt_{pc} electrode in relation to the $Pt_{pc}/Rh_{2.0}/Pt_{1.0}$ electrode (see Table S1 in the Supporting Information for additional values of $\Delta U_m[\Delta(cycles)]^{-1}$ and the total number of cycles). However, instead of comparing the drifts at the same applied current, where the available area of the electrode plays a pivotal role, we conducted the analysis by normalizing the drift in terms of $\Delta U_m[\Delta(cycles)]^{-1}$. With a ratio of approximately 1.2 in the drift, the number of cycles was roughly twice as high in the presence of Pt_{pc}. Remarkably, the same behavior was obtained when the reaction rate of CO_{ad} formation was increased from 1.0 to 5.0. This is a clear evidence that the $Pt_{pc}/Rh_{2.0}/Pt_{1.0}$ electrode does not have a stabilizing effect as observed by Perini et al.,[51] even in the presence of a second metal. The major difference between their experiments and ours is that in our case the second metal is located beneath the platinum outlayer in the $Pt_{pc}/Rh_{2.0}/Pt_{1.0}$ electrode. As the bifunctional mechanism can be discarded in this electrode configuration, the surface oxidation still occurs on platinum active sites, but in this particular situation, the formation of adsorbed carbon monoxide is much slower. Considering that CO_{ad} is the main species responsible for consuming platinum oxides on the surface, formed at high potential values, a lesser number of cycles is expected when the metallic multilayer is used as the working electrode.

The intrinsic drift might also induce morphological changes in period and amplitude simultaneously.[48,63] Figure 5 depicts an amplitude vs period diagram for experiments (filled circles in bold axes) and numerical simulations (open circles in italic
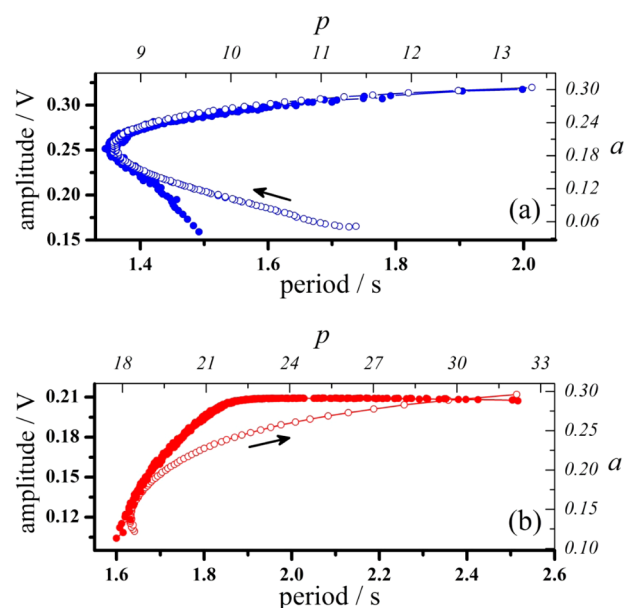
Table 2. Effect of the Metallic Multilayer $Pt_{pc}/Rh_{2.0}/Pt_{1.0}$ and Reaction Rate Constant of CO_{ad} Formation on the Total Number of Oscillatory Cycles[a]

electrode	drift	ratio in drift	no. of cycles	ratio in no. of cycles
		Experiments		
Pt_{pc}	0.130 mV cycle^{-1}	1.11	669	1.64
$Pt_{pc}/Rh_{2.0}/Pt_{1.0}$	0.117 mV cycle^{-1}		406	
Pt_{pc}	0.190 mV cycle^{-1}	1.12	502	2.16
$Pt_{pc}/Rh_{2.0}/Pt_{1.0}$	0.169 mV cycle^{-1}		232	
		Simulations		
$k_2 = 5.0$	2.24×10^{-3}	1.12	132	2.16
$k_2 = 1.0$	2.00×10^{-3}		61	

[a]Simulations considered: $k_1 = 6.0$, $k_3 = 1.0$, $k_4 = 4.0$, $k_5 = 0.079$, $k_6 = 50$, $k_7 = 600$, $k_8 = 30$, $k_9 = 300$, $k_{10} = 0.1$, $\omega = 15$.

Figure 5. Amplitude vs period diagram represented as filled circles for the experiments (amplitude/V vs period/s in bold axes) at $j = 0.64$ mA cm^{-2} and open circles for numerical simulations (a vs p in italic axes): (a) electrochemical reaction on Pt_{pc} and $k_2 = 5.0$ for numerical simulations (blue curves); (b) $Pt_{pc}/Rh_{2.0}/Pt_{1.0}$ and $k_2 = 1.0$ (red curves). The black arrows indicate the direction of an increasing number of cycles from an initial i value of 0.05 and drift of 2.00×10^{-3}. Both simulations consider the values $k_1 = 6.0$, $k_3 = 1.0$, $k_4 = 4.0$, $k_5 = 0.079$, $k_6 = 50$, $k_7 = 600$, $k_8 = 30$, $k_9 = 300$, $k_{10} = 0.1$, and $\omega = 15$.

axes). The blue curves represents the Pt_{pc} electrode and $k_2 =$ 5.0, while the red curves are associated with the $Pt_{pc}/Rh_{2.0}/Pt_{1.0}$ electrode and $k_2 = 1.0$, for electrochemical experiments and numerical simulations, respectively. The surface drift was implemented by slow changes in the applied current with an initial i value of 0.05 and a linear sweep of 2.00×10^{-3}.

Figure 5 shows a typical characteristic of the quadratic relationship between the oscillatory amplitude and bifurcation parameter, along the period drifting: i.e., applied current. As the current is changing slowly with time, we can state the proportional relation amplitude $\propto$ (applied current)$^{1/2}$, which is predicted theoretically.[64] However, differently from Figure 5b, Figure 5a shows a distinct behavior in the onset of the time series. At first, there is an inverse tendency of an increase between the period and amplitude, followed by a concomitant increment after a critical point. In Figure 4, an increase of the applied current resulted in faster oscillations with larger amplitudes. As verified experimentally,[62] larger amplitudes are usually connected with larger periods. A suitable explanation for this dynamic behavior is that higher potential values must be reached in order to promote an effective surface reactivation when the trajectories of the limit cycle have taken a slow excursion in low potentials. Experimental and numerical results[65,66] converge to the idea that poisoning species might block the surface, slowing down the reaction rates. Considering the electro-oxidation of methanol, the consumption of carbon monoxide by oxygenated species is the elementary reaction which mostly influences the oscillatory period.[65] On the basis of this statement, we can clearly make a distinction between parts a and b of Figure 5 by the amount of adsorbed carbon monoxide formed on the surface. The former initially speeds up the formation of carbonaceous intermediates which can be later used in the oxidation of oxygenated species, prolonging the time series and, consequently, the overall number of cycles. Nevertheless, Figure 5b presents a monotonic and gradual decrease by the slow platinum oxidation (see Figure S2 in the Supporting Information for the time evolution of x_4). Similar behavior has been reported in the literature.[48,63]

In summary, the experimental and numerical results described here allow us to propose that a metallic multilayer is indeed a new electrocatalytic material. In the present case, it has improved properties for the electro-oxidation of methanol in acidic solution, leading to important changes in the mechanistic reaction in comparison to that for bulk polycrystalline platinum.

5. CONCLUSIONS

Metallic multilayer electrodes have been utilized as a new kind of nanostructured material with the aim of increasing the catalytic activity in the electro-oxidation of small organic molecules. In this work we provided additional mechanistic evidence of the role played by the $Pt_{pc}/Rh_{2.0}/Pt_{1.0}$ surface in the electro-oxidation of methanol by a combination of electrochemical experiments, modeling, and numerical simulations. A similar voltammetric profile in acidic solutions was observed in both electrodes: i.e., Pt_{pc} and $Pt_{pc}/Rh_{2.0}/Pt_{1.0}$. Remarkably, an increase of about 90% in the peak current density around 0.88 V vs RHE has appeared in anodic linear potentiodynamic sweeps for the $Pt_{pc}/Rh_{2.0}/Pt_{1.0}$ electrode, with respect to that for Pt_{pc}. On the basis of spectroscopic measurements previously reported[10,12] and similar profiles for the hydrogen under-potential deposition in cyclic voltammetriy, the bifunctional mechanism and the formation of rhodium oxides on the surface

can be discarded as being responsible for an increase in the catalytic activity. Consequently, this increase might be attributed solely to the highly selective electronic effect in the prevention of adsorbed carbon monoxide.

Additionally, a considerable increase of period and decrease of amplitude of the oscillations were observed over a wide range of applied current densities and, in contrast to previous studies, the presence of a second metal enhanced the intrinsic drift embedded in the time series. A good qualitative agreement between experiments and simulations was obtained only when lower values of the reaction rate constant of carbon monoxide adsorption were considered in the numerical model. This evidence highlights the effect of metallic multilayer electrodes on the prevention of carbon monoxide layer formation. In other words, carbon monoxide seems to act as a poisoning species instead of a reaction intermediate that contributes to the Faradaic current and total CO_2 production.

■ ASSOCIATED CONTENT

ⓢ Supporting Information

The following file is available free of charge on the ACS Publications website at DOI: 10.1021/cs501652u.

> Simulated voltammetric profiles for i and CO_2 in addition to the time series for CO_{ad} and CO_2 in the electro-oxidation of methanol. The number of cycles and drift in terms of $\Delta U_m[\Delta(\text{cycles})]^{-1}$ measured experimentally under different j values (PDF)

■ AUTHOR INFORMATION

Corresponding Author

*E-mail for E.C.P.: ernesto@ufscar.br.

Present Address

$^{\perp}$(For R.N.) Department of Chemistry, Saint Louis University, 3501 Laclede Ave., St. Louis, MO 63103, USA.

Notes

The authors declare no competing financial interest.

■ ACKNOWLEDGMENTS

■ REFERENCES

(1) Wasmus, S.; Kuver, A. *J. Electroanal. Chem.* **1999**, *461*, 14−31.

(2) Liu, H. S.; Song, C. J.; Zhang, L.; Zhang, J. J.; Wang, H. J.; Wilkinson, D. P. *J. Power Sources* **2006**, *155*, 95−110.

(3) Gurau, B.; Viswanathan, R.; Liu, R. X.; Lafrenz, T. J.; Ley, K. L.; Smotkin, E. S.; Reddington, E.; Sapienza, A.; Chan, B. C.; Mallouk, T. E.; Sarangapani, S. *J. Phys. Chem. B* **1998**, *102*, 9997−10003.

(4) Iwasita, T.; Hoster, H.; John-Anacker, A.; Lin, W. F.; Vielstich, W. *Langmuir* **2000**, *16*, 522−529.

(5) Radmilovic, V.; Gasteiger, H. A.; Ross, P. N. *J. Catal.* **1995**, *154*, 98−106.

(6) Sun, X.; Li, D.; Ding, Y.; Zhu, W.; Guo, S.; Wang, Z. L.; Sun, S. *J. Am. Chem. Soc.* **2014**, *136*, 5745−5749.

(7) Zebarjadi, M.; Shakouri, A.; Esfarjani, K. *Phys. Rev. B* **2006**, *74*, 6.

(8) Johnson, M. T.; Bloemen, P. J. H.; denBroeder, F. J. A.; deVries, J. J. *Rep. Prog. Phys.* **1996**, *59*, 1409−1458.

(9) Bass, J.; Pratt, W. P. *J. Magn. Magn. Mater.* **1999**, *200*, 274−289.

(10) Oliveira, R. T. S.; Santos, M. C.; Marcussi, B. G.; Nascente, P. A. P.; Bulhoes, L. O. S.; Pereira, E. C. *J. Electroanal. Chem.* **2005**, *575*, 177−182.

(11) Oliveira, R. T. S.; Santos, M. C.; Marcussi, B. G.; Tanimoto, S. T.; Bulhoes, L. O. S.; Pereira, E. C. *J. Power Sources* **2006**, *157*, 212−216.

(12) Lemos, S. G.; Oliveira, R. T. S.; Santos, M. C.; Nascente, P. A. P.; Bulhoes, L. O. S.; Pereira, E. C. *J. Power Sources* **2007**, *163*, 695−701.

(13) Freitas, R. G.; Pereira, E. C. *Electrochim. Acta* **2010**, *55*, 7622−7627.

(14) Freitas, R. G.; Pereira, E. C.; Christensen, P. A. *Electrochem. Commun.* **2011**, *13*, 1147−1150.

(15) Freitas, R. G.; Antunes, E. P.; Christensen, P. A.; Pereira, E. C. *J. Power Sources* **2012**, *214*, 351−357.

(16) Zulke, A. A.; Matos, R.; Pereira, E. C. *Electrochim. Acta* **2013**, *105*, 578−583.

(17) Nagao, R.; Cantane, D. A.; Lima, F. H. B.; Varela, H. *Phys. Chem. Chem. Phys.* **2012**, *14*, 8294−8298.

(18) Parsons, R.; Vandernoot, T. *J. Electroanal. Chem.* **1988**, *257*, 9−45.

(19) Cuesta, A. *J. Am. Chem. Soc.* **2006**, *128*, 13332−13333.

(20) Neurock, M.; Janik, M.; Wieckowski, A. *Faraday Discuss.* **2008**, *140*, 363−378.

(21) Strasser, P.; Eiswirth, M.; Ertl, G. *J. Chem. Phys.* **1997**, *107*, 991−1003.

(22) Karantonis, A.; Koutsaftis, D.; Kouloumbi, N. *Chem. Phys. Lett.* **2006**, *422*, 78−82.

(23) Lebedeva, N. P.; Koper, M. T. M.; Feliu, J. M.; van Santen, R. A. *J. Phys. Chem. B* **2002**, *106*, 12938−12947.

(24) Samjeske, G.; Osawa, M. *Angew. Chem., Int. Ed.* **2005**, *44*, 5694−5698.

(25) Osawa, M.; Komatsu, K.; Samjeske, G.; Uchida, T.; Ikeshoji, T.; Cuesta, A.; Gutierrez, C. *Angew. Chem.-Int. Ed.* **2011**, *50*, 1159−1163.

(26) Joo, J.; Uchida, T.; Cuesta, A.; Koper, M. T. M.; Osawa, M. *J. Am. Chem. Soc.* **2013**, *135*, 9991−9994.

(27) Wang, H.; Loffler, T.; Baltruschat, H. *J. Appl. Electrochem.* **2001**, *31*, 759−765.

(28) Wang, H. S.; Baltruschat, H. *J. Phys. Chem. C* **2007**, *111*, 7038−7048.

(29) Abd-El-Latif, A. A.; Baltruschat, H. *J. Electroanal. Chem.* **2011**, *662*, 204−212.

(30) Brimaud, S.; Solla-Gullon, J.; Weber, I.; Feliu, J. M.; Behm, R. J. *ChemElectroChem* **2014**, *1*, 1075−1083.

(31) Delmonde, M. V. F.; Nascimento, M. A.; Nagao, R.; Cantane, D. A.; Lima, F. H. B.; Varela, H. *J. Phys. Chem. C* **2014**, *118*, 17699−17709.

(32) Cuesta, A.; Cabello, G.; Gutierrez, C.; Osawa, M. *Phys. Chem. Chem. Phys.* **2011**, *13*, 20091−20095.

(33) Sauerbrei, S.; Nascimento, M. A.; Eiswirth, M.; Varela, H. *J. Chem. Phys.* **2010**, *132*, 154901.

(34) Nagao, R.; Cantane, D. A.; Lima, F. H. B.; Varela, H. *J. Phys. Chem. C* **2013**, *117*, 15098−15105.

(35) Angerste, H.; Conway, B. E.; Sharp, W. B. A. *J. Electroanal. Chem.* **1973**, *43*, 9−36.

(36) Trasatti, S.; Petrii, O. A. *Pure Appl. Chem.* **1991**, *63*, 711−734.

(37) Liu, P.; Norskov, J. K. *Fuel Cells* **2001**, *1*, 192−201.

(38) Choi, J. H.; Park, K. W.; Park, I. S.; Nam, W. H.; Sung, Y. E. *Electrochim. Acta* **2004**, *50*, 787−790.

(39) Lima, A.; Coutanceau, C.; Leger, J. M.; Lamy, C. *J. Appl. Electrochem.* **2001**, *31*, 379−386.

(40) Gasteiger, H. A.; Markovic, N. M.; Ross, P. N. *J. Phys. Chem.* **1995**, *99*, 8290−8301.

(41) Shubina, T. E.; Koper, M. T. M. *Electrochim. Acta* **2002**, *47*, 3621−3628.

(42) Hammer, B.; Norskov, J. K. *Surf. Sci.* **1995**, *343*, 211−220.

(43) Ruban, A.; Hammer, B.; Stoltze, P.; Skriver, H. L.; Norskov, J. K. *J. Mol. Catal. A: Chem.* **1997**, *115*, 421−429.

(44) Kibler, L. A.; El-Aziz, A. M.; Hoyer, R.; Kolb, D. M. *Angew. Chem., Int. Ed.* **2005**, *44*, 2080−2084.

(45) Rauscher, H.; Hager, T.; Diemant, T.; Hoster, H.; Buatier de Mongeot, F.; Behm, R. J. *Surf. Sci.* **2007**, *601*, 4608−4619.

(46) Narayanamoorthy, B.; Datta, K. K. R.; Eswaramoorthy, M.; Balaji, S. *ACS Catal.* **2014**, *4*, 3621−3629.

(47) Carbonio, E. A.; Nagao, R.; Gonzalez, E. R.; Varela, H. *Phys. Chem. Chem. Phys.* **2009**, *11*, 665−670.

(48) Nagao, R.; Sitta, E.; Varela, H. *J. Phys. Chem. C* **2010**, *114*, 22262−22268.

(49) Lopes, P. P.; Batista, B. C.; Saglietti, G. A.; Varela, H.; Ticianelli, E. A. *J. Solid State Electrochem.* **2013**, *17*, 1851−1859.

(50) Perini, N.; Sitta, E.; Angelo, A. C. D.; Varela, H. *Catal. Commun.* **2013**, *30*, 23−26.

(51) Perini, N.; Batista, B. C.; Angelo, A. C. D.; Epstein, I. R.; Varela, H. *ChemPhysChem* **2014**, *15*, 1753−1760.

(52) Beden, B.; Lamy, C.; Bewick, A.; Kunimatsu, K. *J. Electroanal. Chem.* **1981**, *121*, 343−347.

(53) Beden, B.; Hahn, F.; Juanto, S.; Lamy, C.; Leger, J. M. *J. Electroanal. Chem.* **1987**, *225*, 215−225.

(54) Kunimatsu, K.; Kita, H. *J. Electroanal. Chem.* **1987**, *218*, 155−172.

(55) Iwasita, T. *Electrochim. Acta* **2002**, *47*, 3663−3674.

(56) Batista, E. A.; Malpass, G. R. P.; Motheo, A. J.; Iwasita, T. *J. Electroanal. Chem.* **2004**, *571*, 273−282.

(57) Batista, E. A.; Malpass, G. R. P.; Motheo, A. J.; Iwasita, T. *Electrochem. Commun.* **2003**, *5*, 843−846.

(58) Housmans, T. H. M.; Wonders, A. H.; Koper, M. T. M. *J. Phys. Chem. B* **2006**, *110*, 10021−10031.

(59) Chen, Y. X.; Miki, A.; Ye, S.; Sakai, H.; Osawa, M. *J. Am. Chem. Soc.* **2003**, *125*, 3680−3681.

(60) Reichert, R.; Schnaidt, J.; Jusys, Z.; Behm, R. J. *ChemPhysChem* **2013**, *14*, 3678−3681.

(61) Reichert, R.; Schnaidt, J.; Jusys, Z.; Behm, R. J. *Phys. Chem. Chem. Phys.* **2014**, *16*, 13780−13799.

(62) Mota, A.; Lopes, P. P.; Ticianelli, E. A.; Gonzalez, E. R.; Varela, H. *J. Electrochem. Soc.* **2010**, *157*, B1301−B1304.

(63) Cabral, M. F.; Nagao, R.; Sitta, E.; Eiswirth, M.; Varela, H. *Phys. Chem. Chem. Phys.* **2013**, *15*, 1437−1442.

(64) Strogatz, S. H. *Nonlinear Dynamics and Chaos: With Applications to Physics, Biology, Chemistry, and Engineering*; Addison-Wesley: Cambridge, MA, 1994.

(65) Batista, B. C.; Ferreira, G. C. A.; Varela, H. *J. Phys. Conf. Ser.* **2011**, *285*, 012003.

(66) Ferreira, G. C. A.; Batista, B. C.; Varela, H. *PLoS One* **2012**, *7*, e50145.